Article ID: 1006-8775(2010) 03-0247-08

A NUMERICAL STUDY OF TROPICAL DEEP CONVECTION USING WRF MODEL

LI Jia-peng (李嘉鹏)[1,2], YIN Yan (银　燕)[1], JIN Lian-ji (金莲姬)[1], ZHANG Cheng-zhu (张成竹)[1]

(1. CMA Key Laboratory for Atmospheric Physics and Environment, Nanjing University of Information Science & Technology, Nanjing 210044 China; 2. Zhejiang Meteorological Observatory, Hangzhou 310017 China)

Abstract: The Weather Research Forecast model (WRF) configured with high resolution and NCEP 1°×1° reanalysis data were used to simulate the development of a tropical deep convection over the Tiwi Islands, northern Australia, and to investigate the sensitivity of model results to model configuration and parameterization schemes of microphysical processes. The simulation results were compared with available measurements. The results show that the model can reproduce most of the important characteristics of the observed diurnal evolution of the convection, including the initiation of convection along the sea-breeze front, which is then reinforced by downdraft outflows, merging of cells and the formation of a deep convective system. However, further improvement is needed to simulate more accurately the location and the time for initiation of the deep convective system. Sensitivity tests show that double-nesting schemes are more accurate than the non-nesting schemes in predicting the distribution and intensity of precipitation as far as this particular case is concerned. Additionally, microphysical schemes also have an effect on the simulated amount of precipitation. It is shown that the best agreement is reached between the simulation results and observations when the Purdue Lin scheme is used.

Key words: tropical deep convection; WRF model; parameterization of microphysical processes; nesting; sensitivity experiment

CLC number: P435 **Document code:** A **doi:** 10.3969/j.issn.1006-8775.2010.03.006

1 INTRODUCTION

Tropical deep convection (TDC) provides the primary mechanism whereby solar heating received by the tropical ocean is carried upward into the free troposphere where it can be transported poleward. During this process, these great engines of the global climate produce precipitation and drive the global-scale circulation. The reactions between TDC and large-scale circulations determine the clouds, moisture, temperature and structure of the troposphere in tropical regions. In addition, TDC is the source of water vapor for the upper troposphere in the tropics. The upper-tropospheric moisture provided by TDC plays an important role in maintaining the natural greenhouse effect in the atmosphere[1]. Observations from geostationary satellites show that TDC have distinct diurnal cycles. Meanwhile, TDC can transport air, which contains various trace gases and aerosol components, from lower boundary layer to upper troposphere, even to the lower stratosphere in a short time[2]. The effect on the chemical properties of the upper troposphere and lower stratosphere (UTLS) of the transported atmospheric chemical compounds has attracted much attention during the last few decades and a series of internationally collaborated field campaigns were conducted to investigate the impact of TDC on the vertical redistribution of chemicals and moisture in the tropical region.

Recently, an international project named ACTIVE (Aerosal and Chemical Transport In Tropical Convection) cooperated among Britain, Canada, Australia and other countries was conducted on Tiwi Islands, northern Australia, to investigate the effect of TDC on the chemical composition of the tropical tropopause layer (TTL). The Tiwi Islands consist of two small and flat islands, Melville (M) to the east, and Bathurst (B) to the west. They are located at 11°S, and are 50 to 100 km away from the northwest point of

Received date: 2009-11-24; **revised date:** 2010-05-10
Foundation item: National Natural Science Foundation (40675005); Science Foundation (QD52); Natural Science Foundation for High Education in Jiangsu Province (06KJB170047)
Biography: LI Jia-peng, M.S. candidate, primarily undertaking research on interactions of cloud physics.
E-mail for corresponding author: yinyan@nuist.edu.cn

Australian continent. The highest altitude of the islands is about 100 meters above sea level. The two small islands are separated by the Apsley channel. A TDC system, named Hector by the local residents, occurs almost everyday during the transitional season (November to December) and monsoon break periods. The relatively flat topography and the regularity of the occurrence of Hector make Tiwi islands an ideal place to observe TDC.

A handful of observational and numerical studies have been conducted to understand the development and structure of Hector. It was commonly believed that the Hector clouds were triggered by collision of the sea breeze from two sides of the Tiwi islands. With analysis of the Doppler radar data obtained during the MCTEX (Maritime Continent Thunderstorm Experiment) project, it was found, however, that collisions between the sea breezes rarely occur. Based on these findings, Carbone et al.[3] classified the development of convection over the Tiwi islands into two types: The type A mode, which accounts for about 20% of the total convection, is triggered by the interaction of the sea breezes from two sides of the island; the type B mode, which accounts for the remaining 80%, represents the strongest convection triggered by the interactions between sea breeze and gust fronts produced by earlier weak convection. It is also indicated that the type A mode always occurs under relatively stable atmospheric conditions which can make the sea breeze go deep into the central area of the islands. By analyzing different data from ITEX (Island Thunderstorm Experiment) project, Keenan et al.[4] showed that the evolution of dynamic structure of Hector, such as the lower-level wind-shear and the allocation of CAPE (convective available potential energy) and moisture content, was quite similar to the general feature of multi-cell convective systems.

Golding et al.[5] used the mesoscale model of UK. Met. Office and simulated two cases observed during ITEX. They reproduced the development of the TDC over the Tiwi islands, but the 3-km resolution and a single sounding thermodynamic profile used in their simulation, however, were unable to resolve the fine structure of the clouds. Satio et al.[6] simulated a tropical convection observed during MCTEX with the double-nested 1-km resolution MRI NHM. The results demonstrated that the diurnal evolution of the convection is characterized by a transition from horizontally forced convection in the morning to a vertical convection in the afternoon. They classified the life cycle into five stages: 1) The dry stage. During this stage a sea breeze front driven by the temperature difference between the sea and land appears along the seashore, and Rayleigh-Benard convection develops over the inner island. Meanwhile, horizontal convective rolls oriented along the direction of sea breezes may appear, especially at the windward coast. 2) The condensation stage. During this stage, upward motion at the sea breeze front head and Rayleigh-Benard cells exceed the lifting condensation level (LCL) and shallow clouds appear along the sea breeze front. The release of latent heat is small at this stage and the basic circulation over the island is the same as in the first stage. 3) The precipitation stage. During this stage, sea breeze from both sides intrude farther inland; meanwhile, upward motion in some clouds becomes stronger, and precipitation begins to appear at the surface. Clouds align along the leeside coast of the islands and the sea breeze propagates further inland without the formation of distinct cloud lines at the windward coast. The sea breeze forms a convergence zone, where the Rayleigh-Benard convection cells become less distinct, near the central area of the island. 4) The merging stage. Cloud lines form on the lee side of the islands in an east-west direction; meanwhile, deep convection begins to form with cloud merging. 5) The decay stage. Convection decays gradually with the decrease of solar radiation.

All the studies mentioned above used a single sounding profile as the initial condition to simulate TDCs and stated that the results were representative of the development and mechanisms of convection. However, the lack of large scale meteorological background limited their results for general representation of TDCs. In this study, the latest version of WRF model with high resolution (1°×1°) NCEP reanalysis data was used to simulate the development of TDCs and to investigate the influence on cloud development of different model configurations. Section 2 gives a general introduction to the model and simulation configuration. Analysis of the observed as well as the simulated convection will be given in Section 3. The simulation results using different configurations will be presented in Section 4, followed by conclusions in Section 5.

2 THE MODEL AND THE EXPERIMENTS

WRF model is a new-generation high computational efficiency mesoscale forecast and assimilation system which can support 1-way and 2-way multi-domain nesting. This model focuses on the application of forecast and research from cloud to synoptic scale and provides several parameterization schemes[7-8]. A lot of work has been done on forecast and research using WRF model all over the world. Sun et al.[9] simulated three heavy rain events in 1998 in China using WRF and MM5 models respectively, and showed that for all levels of heavy rain processes and in all areas, the accuracy of simulated weather systems

and rainfall areas using WRF is superior to that of MM5 except that the amount of the precipitation is less than the observations. However, Hou[10] simulated 11 heavy rain events in Shanxi in 2005 using three-domain nesting configuration, and demonstrated that the precipitation amount was overestimated in the simulations. Wang et al.[11] found that the rainfall intensity and area were simulated more realistically when nested domains were used. On the other hand, Holland and Leung et al.[12, 13] simulated tropical atmospheric circulation using WRF model with 4-km resolution and found that the model presented a good performance on reproducing the monsoon circulation in the Australian area. Wapler[14] also simulated a convection that occurred in the Darwin area during the TWP-ICE project using 1.3-km resolution and evaluated the simulation results with observational data.

In this study, the WRF model version 2.1.2[15] and NCEP 1°×1° global analysis data were used to simulate a deep convection that occurred over the Tiwi islands on November 16, 2005, and to understand the effects on model results of horizontal resolution and nested configuration. The model domain is shown in Fig. 1. Four cases were examined in this paper (Table 1): Cases 1 and 2 were set up with 1 and 2 km horizontal resolutions, respectively; Cases 3 and 4 were configured with nested double-domain with a coarse grid size of 3 km and a fine grid of 1 km, respectively. Cases 1, 2 and 3 used the same schemes for parameterization of cloud microphysical processes, PBL and radiative processes to evaluate the influence of resolution and nested configuration on simulation. The Purdue Lin scheme, which is a relatively more sophisticated scheme and includes five hydrometer species of cloud, rain, ice, snow and grauple, was chosen for Cases 1, 2 and 3 in the microphysical processes. This scheme was first presented by Lin et al.[16] and was improved by Rutledge and Hobbs[17] and Tao et al.[18]. The WSM6 microphysics scheme, which is similar to Purdue Lin scheme but with different calculation of the amount of hydrometer, was used in Case 4 in order to evaluate the influence of microphysical schemes. In all the cases, explicit cumulus scheme, instead of cumulus parameterization, was used. The integration was conducted from 0630 LST to 2130 LST on November 16, 2005 with a time step of 10 seconds. In addition, 31 sigma levels in the vertical direction were considered in all the cases. The radar observations from ACTIVE project in the Darwin area were used to evaluate the simulation results.

3 GENERAL FEATURE OF THE TDC CASE

A typical TDC (Hector) that occurred over Tiwi islands on November 16, 2005 was considered in this study. The sounding data (Fig. 2) presents a typical unstable vertical profile in this season and implies that strong convection would occur later that day.

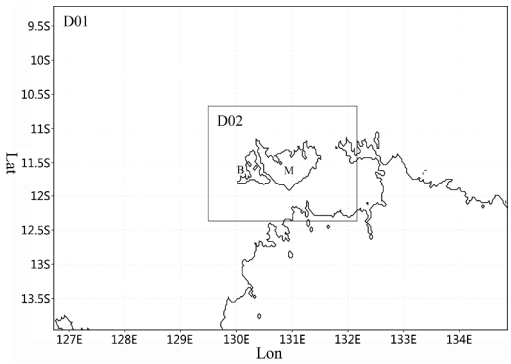

Fig.1. Model domain (B is short for Bathurst island and M is for Melville island)

Table 1. Schemes For numerical experiments

Schemes	Horizontal grid intervals	Microphysics
Case 1	1 km	Purdue Lin
Case 2	2 km	Purdue Lin
Case 3	Course 3 km, fine 1 km	Purdue Lin
Case 4	Course 3 km, fine 1 km	WSM6

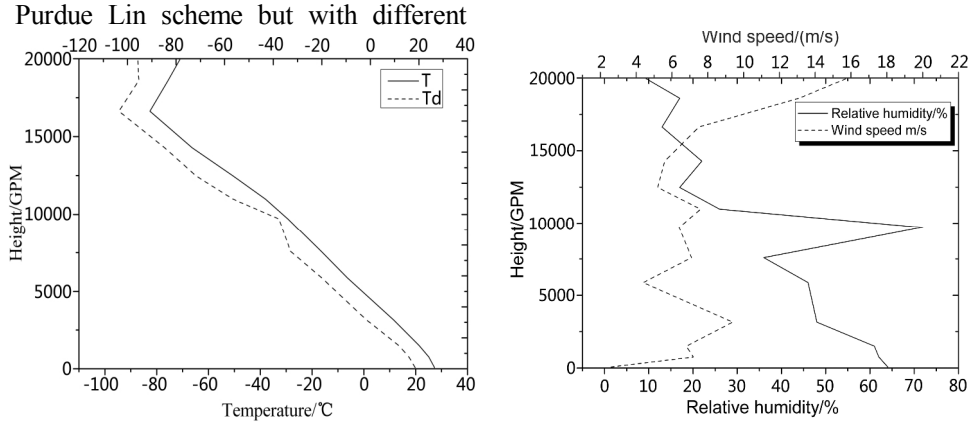

Fig. 2. Sounding profiles at Darwin station. Left panel: temperature (solid) and dew point temperature (dotted); right panel: relative humidity (solid) and wind speed (dotted)

Figure 3 shows the cloud images over Tiwi islands derived from GMS satellite. The sky was almost clear in the morning. Then, the inner island began to be covered by shallow convective clouds starting from 1230 LST (Fig. 3, left panel), and two hours afterwards the clouds began to enhance and arranged as a cloud line in E-W direction along the southern coast region. Furthermore, these shallow convective clouds merged and formed a stronger convection in the southern central area of M island and the central area of B island. At last, these deep convective clouds moved to the southwest and disappeared gradually after 1600 LST.

Figure 4 shows the precipitation process observed by the Doppler radar in Darwin. At 1158 LST it began to rain at Pirlangimpi station at the west rim of M island. The rain then moved to the central region of M island and spread over the whole western part of it. At the same time, the convection became stronger. The rainfall on B island started at 1400 LST and then merged with the system over M island. A relatively strong rainfall sustained from 1500 LST to 1600 LST in both the southern and western part of M island and southern and central area of B island. After 1630 LST, the core rainfall area gradually moved to the southwest of B island. Meanwhile, moderate precipitation was observed at Nguiu station on M island and a second round of precipitation was observed at Pirlangimpi station. Finally, the rainfall around the islands ceased after 1800 LST.

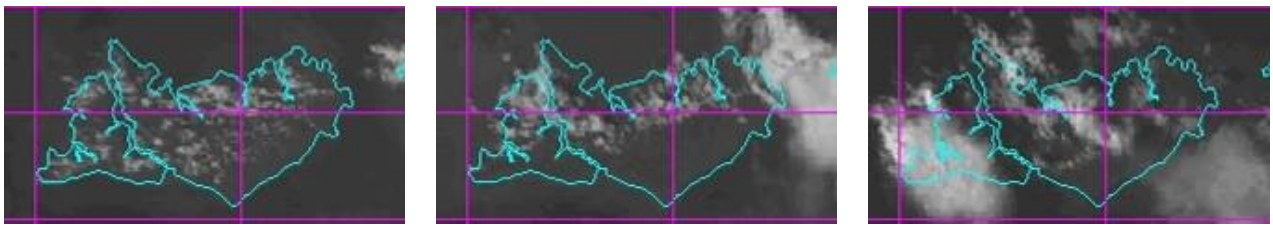

Fig. 3. GMS visible images at 1230 LST (left panel), 1430 LST (middle panel) and 1600 LST (right panel) November 16, 2005

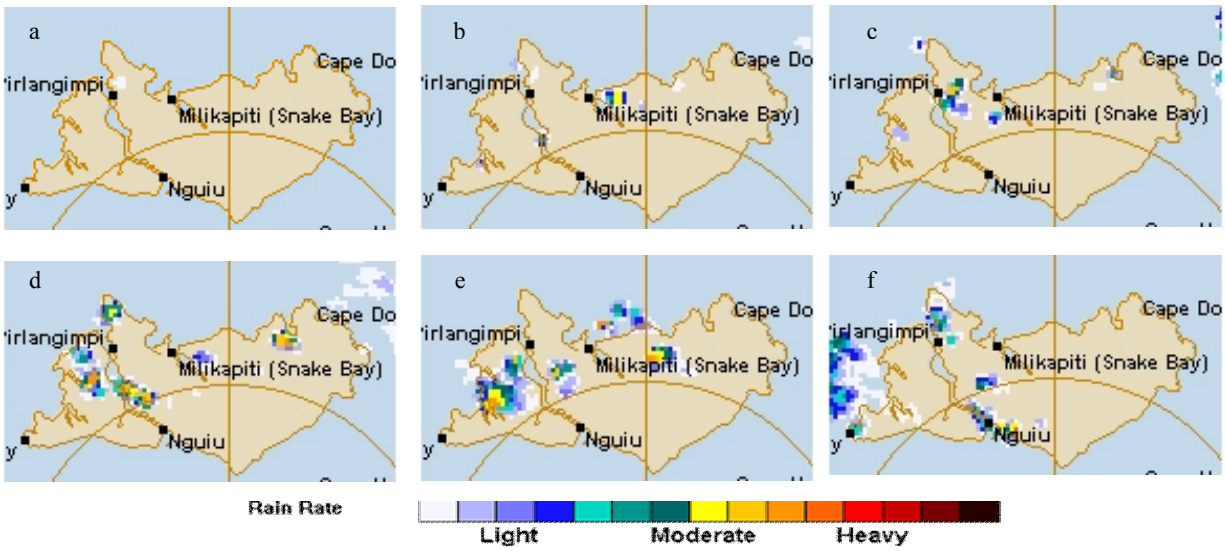

Fig. 4. Surface rainfall intensity estimated by radar observation at 1200 LST (a), 1300 LST (b), 1400 LST (c), 1500 LST (d), 1600 LST(e) and 1700 LST(f) on November 16, 2005

4 MODEL RESULTS AND DISCUSSIONS

4.1 *Development of the convection*

The simulation results of Case 3 are used here to demonstrate the evolution of the convection. Figure 5 shows the horizontal wind field at 10 m and the vertical velocity field at 100 m. Because of the solar radiation heating, 2–3 m/s sea breezes initiated along the coasts of the islands and formed a sea breeze front. Meanwhile, some shallow convective clouds emerged along the sea breeze front, especially in the north-coast region where relatively strong convection occurred due to the convergence produced by high terrain. We denote this period as the development phase of the convection. Most of the shallow convective clouds occurring during this period have single-cell structure (Fig. 6).

These single shallow convective clouds differed from each other in the development processes and began to merge and to precipitate when the sea breezes went deeper into the inner area of the island. We denote this period as the merging phase (Fig. 7). In the merging phase, a number of convective clouds merged to form stronger convection. Meanwhile, these

formerly single-cell convective clouds started to disappear and new cells were triggered by the environmental air flow and the downdraft produced by these convective clouds. Multi-cell storms produced local heavy rainfall and moved slowly.

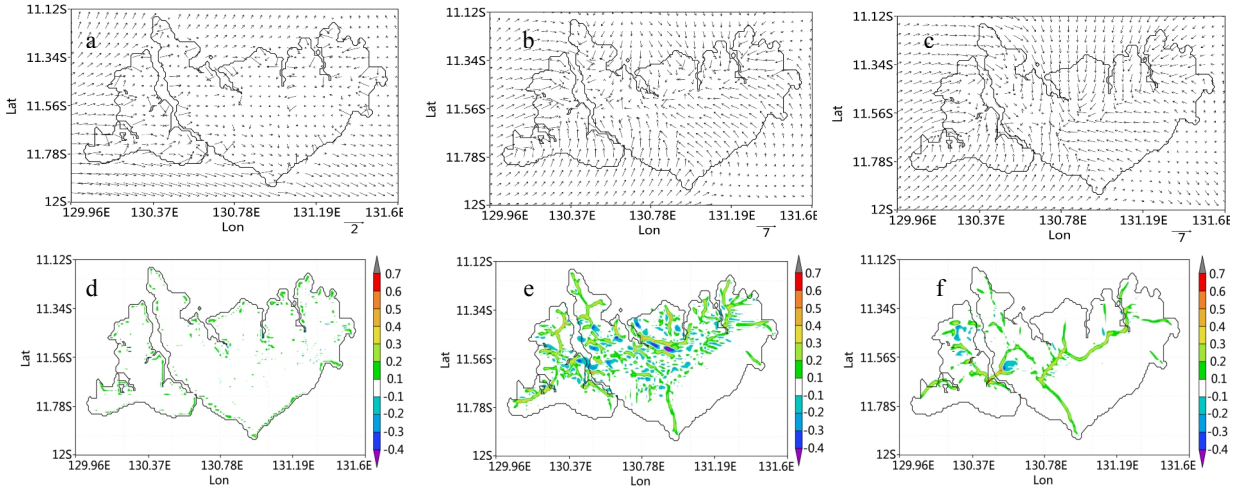

Fig. 5. Simulated 10-m horizontal wind field (a, b, c) and 100-m vertical velocity (d, e, f) at 0900 LST, 1300 LST and 1700 LST

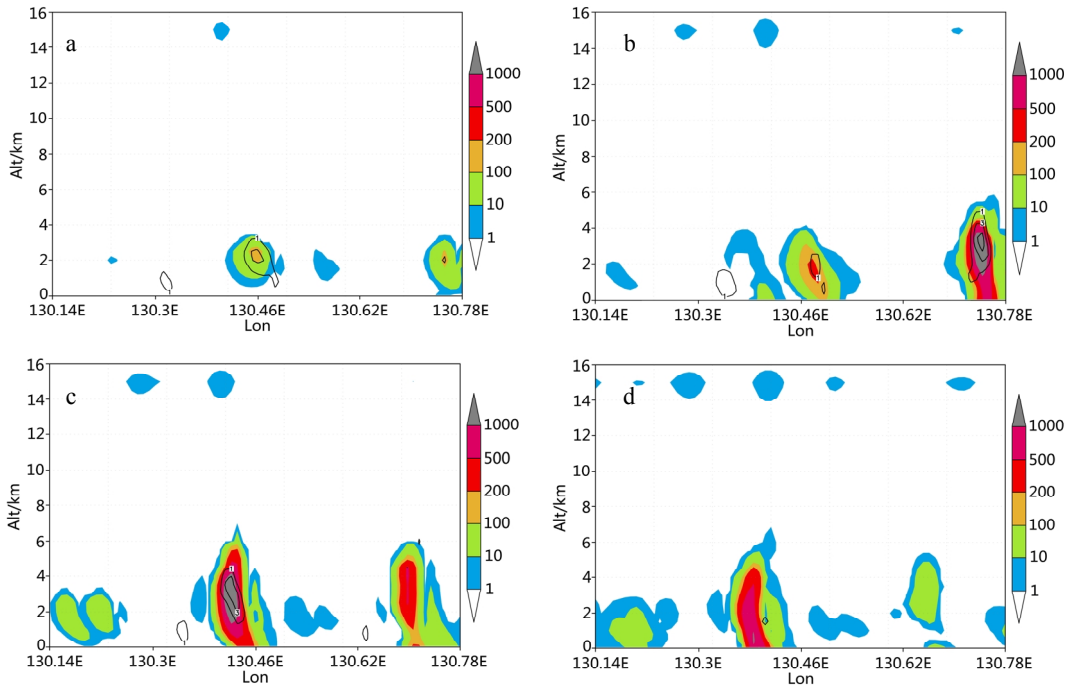

Fig. 6. Simulated cross-section of total water content (shaded, units: mg/kg) and vertical velocity (contour, units: m/s) along 11.40°S and at 1240 LST (a), 1300 LST (b), 1310 LST (c) and 1320 LST (d)

The simulation showed that single-cell convective clouds started to merge and form a multi-cell convection which led to heavy precipitation after the earlier rainfall caused by prior shallow convective cells. Figure 7 gives the merging and moving processes of typical single-cell convective clouds: two typical single-cell convection, with cloud tops reaching 8 km and 5 km, respectively, initiated at the west area of M island at 1530 LST, then merged into a single convection with its cloud top reaching 9 km and the maximum intensity of the vertical velocity in the central area of the cloud body reaching more than 9 m/s.

Figure 8 shows the total water content and vertical velocity at the strongest convection period at 1700 LST. Convection grew up rapidly, and the cloud top reached 14 km and spread around and formed an anvil at the upper levels. The maximum total water content reached more than 1.0 g/kg and a large area was covered by the clouds.

Droegemeier et al.[19] and Simpson et al.[20] proposed that new convection can be triggered by the downdraft produced by previous convection, but the case simulated here does not show that mature

convection could cause a new and stronger convection.

The simulated precipitation, which mainly distributed around Apsley channel, initiated at 1220 LST in some single-cell convective clouds and became heavier at 1510 LST. Furthermore, the precipitation field moved to the west and the core of precipitation field arrived at the west rim of M island at 1550 LST. Comparing with the observations, one can find that the model has relatively good capability to simulate the precipitation event except for the rainfall area. The simulated appearance of the strongest convection is delayed for about one hour. In addition, the simulated distribution of cloud body was consistent with the observations that most convective clouds are mainly arranged along the E-W line across the Apsley channel and then moved to the west area, except that a relatively strong convection occurring at the northeast area of M island is missed by the model.

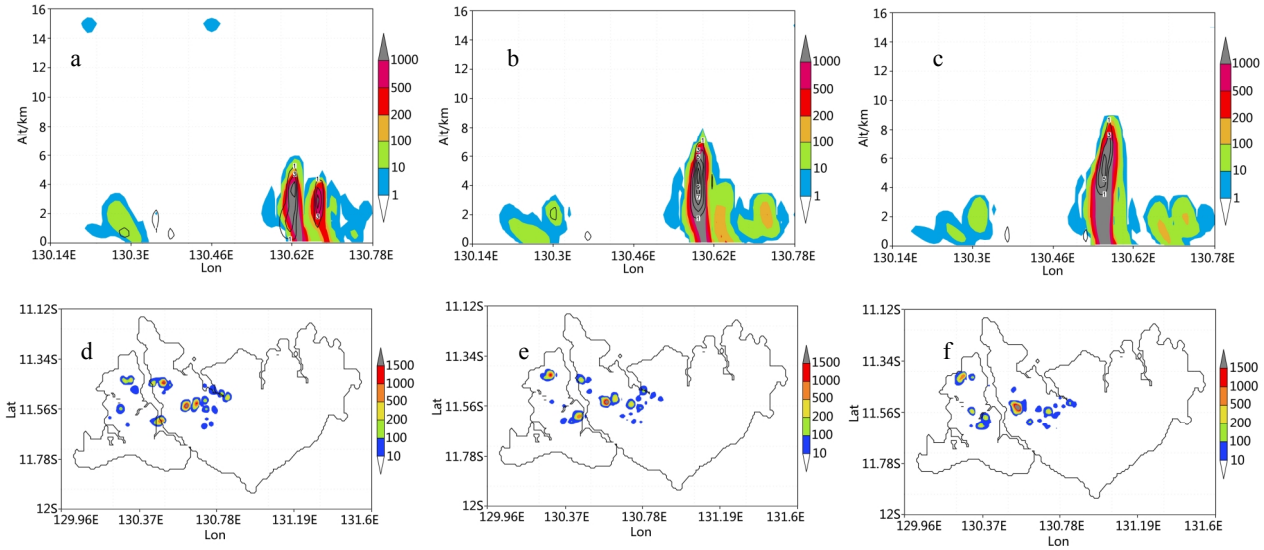

Fig. 7. Simulated cross-section of total water content (shaded, units: mg/kg) and vertical velocity (contour, units: m/s) along 11.55°S at 1530 LST (a), 1540 LST (b), 1550 LST (c) and 2.5 km total water content (units: mg/kg) at the corresponding time (d, e, f)

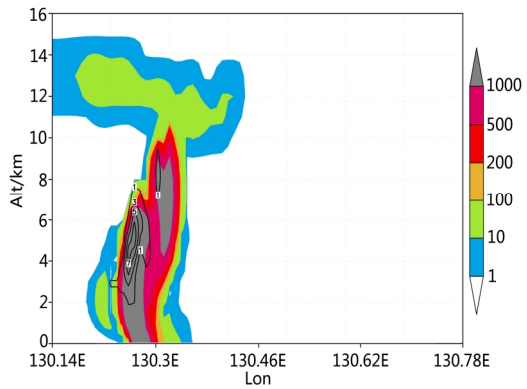

Fig. 8. Simulated cross-section of total water content (shaded, units: mg/kg) and vertical velocity (contour, units: m/s) of the strongest convection along 11.46°S at 1700 LST.

After 1700 LST, the core area of the convective system moved from the central region of B island to the west and precipitation began to decrease. The atmospheric profile became more stable due to the release of unstable energy and decrease of short wave radiation intensity.

Meanwhile, the anvil at the upper level spread to southwest under the influence of the upper level wind.

Based on the above analysis, the simulated location and intensity of the strongest convection have relatively good agreement with the observations, but the capacity of the model to simulate the appearance time is limited. This may be caused by the random characteristic of convection and the lack of accuracy of initial meteorological fields.

From the results one can find that the initial convection was triggered by sea breezes and went deep into the inner area of island together with the sea breeze front, and at the same time, convective clouds acquired energy from the sea breeze front continuously. Furthermore, the phenomenon that the intensity of convection enhanced remarkably after crossing the channel demonstrates that the precipitation could be influenced significantly by the topography.

4.2 *Comparison of the results using different resolutions and nesting domains*

The rainfall time in Cases 1, 2 and 3 are 1400–800 LST, 1500–810 LST and 1220–800 LST, respectively, indicating that the result of Case 3 was most similar to the observations among the three cases and that the rainfall was delayed in Cases 1 and 2. Figure 9 shows the core area and distribution of precipitation from

different cases. Case 1 only simulated small amount of rainfall at the central area of B island and west area of M island, while Case 2 just reproduced a smaller rainfall area at the west area of M island. The rainfall distribution in Case 3 is most similar to the observations. However, some precipitation was still underestimated at Nguiu station.

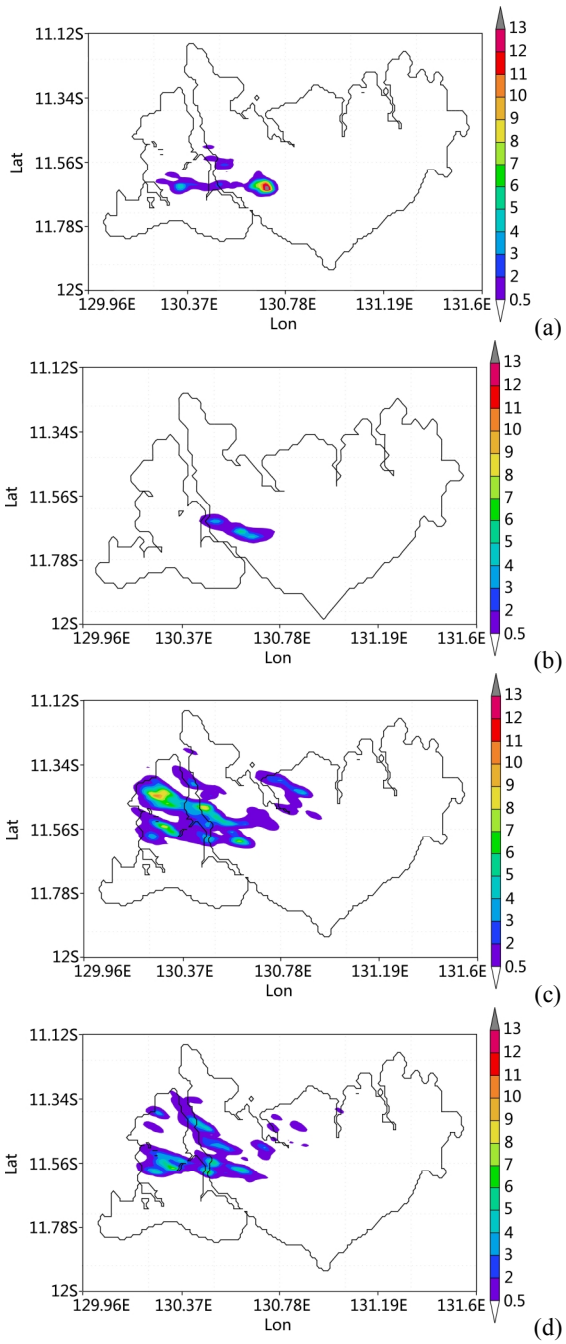

Fig. 9. Simulated distribution of total precipitation with Case 1 in (a), Case 2 in (b), Case 3 in (c) and Case 4 in (d), respectively (units: mm)

The total precipitation and rainfall intensity in different cases differ greatly. Case 1 shows a weaker rainfall area at the central region of B island and a relatively stronger rainfall area at the west coast of M island (Fig. 9a), and the maximum precipitation exceeds 12 mm. Case 2 only gives one rainfall area at the west coast of M island with the maximum precipitation of 6 mm. Due to the lack of observational precipitation data, we could not evaluate more quantitatively the capability of the model in simulating precipitation. However, comparisons of the radar-observed rainfall intensity and distribution suggest that simulation with nested domain can produce a relatively larger rainfall area at the north region of B island with the maximum precipitation of 12 mm, indicating that the best agreement between simulated and observed total precipitation can be reached using this configuration.

4.3 *Comparison of the results using different microphysical parameterizations with nesting domains*

Previous studies proposed that microphysical parameterization schemes could influence the effect of simulated precipitation obviously[16]. Sensitivity experiments carried out using two schemes in this study prove the above conclusions to certain extent. Both of the two different schemes reproduce the rainfall at the central area of B island and the west coast of M island, but some differences are still found according to rainfall intensity and distribution. The results simulated using Lin scheme (Fig. 9c), which reproduces an obvious rainfall core at the north area of B island, were closer to the observation. The comparison of the rainfall simulation using WSM6 scheme (Fig. 9d) and Lin scheme demonstrated that different assumptions of microphysical processes and various calculating methods of hydrometers could lead to differences in rainfall distribution and intensity, although these two schemes had similar classification setup for hydrometers.

5 CONCLUSIONS

The WRF model was used to simulate the development of a tropical deep convection over the Tiwi Islands, northern Australia, and to investigate the sensitivity of model results to model resolution and microphysical parameterization schemes. The simulation results were compared with available measurements. The results show that the model could reproduce the most important characteristics of the observed diurnal evolution of the convection, including the initiation of convection along the sea breeze front which was then reinforced by downdraft outflows, merging of cells and the formation of a deep convective system. Sensitivity tests show that double-nesting schemes are more accurate than the non-nesting

schemes in predicting the distribution and intensity of precipitation as far as this particular case is concerned. Additionally, microphysical schemes also had some impacts on the simulation of precipitation. Better agreement is reached between the simulation results and observations when the Purdue Lin scheme is used. However, the WRF model still has some limitations on simulating relatively small local convection, especially on accurately simulating the location and time for deep convection.

REFERENCES:

[1] HARTMANN D L. Tropical Convective Clouds [EB/OL] [2007-04-05]. http://eos.atmos.washington.edu.
[2] DING Yi-hui, WANG Zhun-ya, SONG Ya-fang et al. Cause of the unprecedented freezing disaster in January 2008 and its possible association with the global warming [J]. Acta Meteor. Sinica, 2008, 66(5): 808-825.
[3] ZHAO Si-xiong, SUN Jian-hua. Multi-scale systems and conceptual model on freezing rain and snow storm over southern China during January-February 2008 [J]. Climat. Environ. Res., 2008, 13(4): 351-367.
[4] LI Chong-yin, YANG Hui, GU Wei. Cause of severe weather with cold air, freezing rain and snow over south China in January 2008 [J]. Climate Environ. Res., 2008, 13 (2): 113-122.
[5] GU Lei, WEI Ke, HUANG Rong-hui. Severe disaster of blizzard, freezing rain and low temperature in January 2008 in China and its association with the anomalies of East Asia monsoon system [J]. Climate Environ. Res., 2008, 13(4): 405-418.
[6] WANG Dong-hai, LIU Chong-jian, LIU Ying, et al. A preliminary analysis of features and causes of the snow storm event over the Southern China in January 2008 [J]. Acta Meteor. Sinica, 2008, 66(3): 405-422.
[7] WANG Shao-wu. Climatological aspects of severe winters in China [J]. Adv. Climate Change Res., 2008, 4(2): 68-72.
[8] LIU Chao-feng, CHEN Hong, LIN Zhao-hui. Numerical simulation of the impact of sea surface temperature anomalies on the climate anomalies over China in January 2008 [J]. Climat. Environ. Res., 2008, 13(4): 500-509.
[9] ZONG Hai-feng, ZHANG Qing-yun, BUHE Cho-law, et al. Numerical simulation of possible impacts of Kuroshio and North Atlantic sea surface temperature anomalies on the South China snow disaster in January 2008 [J]. Climate Environ. Res., 2008, 13 (4): 491-499.
[10] FU Jian-jian, LI Shuang-lin, WANG Yan-ming. Influence of prior thermal state of global oceans on the formation of the disastrous snow storm in January 2008 [J]. Climate Environ. Res., 2008, 13 (4): 479-490.
[11] COLLINS W D, RASCH P J, et al. Description of the NCAR Community Atmosphere Model (CAM3.0) [R]// Technical Report NCAR/TN-464+ STR, Boulder: National Center for Atmospheric Research, 2004, 216pp.
[12] CHEN Hai-shan, SUN Zhao-bo, NI Dong-hong, et al. Numerical experiments on the responses of East Asian winter monsoon to autumn and winter SSTA [J]. J. Nanjing Inst. Meteor., 2002, 25(6): 721-730.
[13] DONG Min. Validation study on the East Asian climate simulated by CCM2 [J]. Acta Meteor. Sinica, 1997, 55(1): 692-702.
[14] TANG Ming-min, ZENG Wen-hua, HE Yuan. The influence of the summer SSTA of the eastern hemispheric tropical season the Asian monsoon circulation and precipitation- a numerical experiment [J]. J. Trop. Meteor., 1993, 9(4): 289-298.
[15] XU Hai-ming, HE Jing-hai, DONG Min. Interannual variability of the Meiyu onset and its association with north Atlantic oscillation and SST anomalies over north Atlatic [J]. Acta Meteor. Sinica, 2001, 59(6): 694-706.
[16] SMITH T M, REYNOLDS R W. Improved extended reconstruction of SST (1854-1997) [J]. J. Climate, 2004, 17: 2466-2477.
[17] HE Xi-cheng, DING Yi-hui, HE Jin-hai. Response characteristics of the East Asian winter monsoon with ENSO events [J]. Chin. J. Atmos. Sci., 2008, 32(2): 335-344.
[18] BLACKMON M L. A general circulation model study of January climate anomalous Patterns associated with interannual variation of equatorial Pacific sea surface Temperature [J]. J. Atmos. Sci., 1983, 40 (6): 1 410-1 425.
[19] SHUKLA J, WALLACE J M. Numerical simulation of the atmospheric response to Pacific SST anomalies [J]. J. Atmos. Sci., 1983, 40(7): 1 613-1 630.
[20] CHEN Lie-ting. Features of atmosphere circulation related to global weather abnormal and its relation with sea surface temperature [J]. Chin. Sci. Bull., 1974, 19(8): 372-375.
[21] WU Guo-xiong, WANG Jing-fang. Comparison of the correlations of lower tropospheric circulation with tropical and extratropical sea surface temperature anomalies [J]. Acta Meteor. Sinica, 1996, 54(4): 387-397.
[22] WALLACE J M, GUTZLER D S. Teleconnection in the geopotential height field during the Northern Hemisphere winter [J]. Mon. Wea. Rev., 1981, 109(4): 784-812.
[23] GAMBO K, KUDO K. Three dimensional teleconnections in the zonally asymmetric height field during the Northern Hemisphere winter [J]. J. Meteor. Soc. Japan, 1983, 61: 36-52.
[24] LI Shuang-lin. Impact of northwest Atlantic SST anomalies on the circulation over the Baikal Mountains during early winter [J]. J. Meteor. Soc. Japan, 2004, 82(4): 971-988.
[25] YANG Jian-ling, LIU Qin-yu. The “charge/discharge” roles of the basin-wide mode of the Indian Ocean SST anomaly—influence on the South Asian High in summer [J]. Acta Oceanol. Sinica, 2008, 30(2): 12-19.
[26] MATSUNO T. Quasi-geostropic motions in the equatorical area [J]. J. Meteor. Soc. Japan, 1966, 44, 25-43.
[27] GILL A E. Some simple solutions for heat-induced tropical circulation [J]. Quart. J. Roy. Meteor. Soc., 1980, 106 (449): 447-462.

Citation: LI Jia-peng, YIN Yan, JIN Lian-ji et al. A numerical study of tropical deep convection using WRF model. *J. Trop. Meteor.*, 2010, 16(3): 247-254.